Asian Journal of Chemistry; Vol. 38, No. 6 (2026), 1641-1651
ASIAN JOURNAL OF CHEMISTRY
https://doi.org/10.14233/ajchem.2026.35704

Biowaste-Derived Gold Nanoparticles: Synthesis Optimisation, Characterisation and Biomedical Potential

RAMESH BABU KONAKALA[1], NIRMALA RAJKUMAR[1,*], KIRAN KUMAR KODURI[1], RANGASWAMY NAVAMATHAVAN[2] and JAISANKAR VISWANATHAN[3]

[1]PG and Research Department of Biotechnology, Hindustan College of Arts and Science (Affiliated to University of Madras), Padur, Chennai-603103, India
[2]Department of Physics, School of Advanced Sciences, Vellore Institute of Technology (VIT), Chennai-600127, India
[3]Department of Chemistry, Presidency College (Autonomous), Chennai-600005, India

*Corresponding author: E-mail: drrnirmala@hcaschennai.edu.in

Received: 4 February 2026 *Accepted*: 23 May 2026 *Published online*: 31 May 2026 AJC-22391

Biowaste-derived gold nanoparticles (Au NPs) provide a cost-effective and environmentally beneficial substitute for conventional chemical synthesis methods. In this study, Au NPs were synthesised using biowaste fruit peel extracts rich in bioactive compounds, serving as reducing and stabilizing agents. Around six peel extracts from various fruits (*Malus pumila*, *Musa paradisiaca*, *Citrus sinensis*, *Vitis vinifera*, *Punica granatum* and *Persea americana*) were screened for synthesis processes. Among these, *M. pumila* (apple) peel extract was selected for further study due to its superior nanoparticles formation efficiency. The synthesised Au NPs were characterised to confirm their structural, morphological and optical properties. The optimisation of synthesis parameters, including pH, temperature, precursor concentration and volume of peel extract was conducted to achieve monodispersed and stable Au NPs. The synthesised Au NPs exhibited significant antioxidant activity, as assessed by DPPH, ABTS and FRAP assays, demonstrating their potential in scavenging free radicals. Furthermore, the cytotoxicity of Au NPs was evaluated against breast cancer MDA-MB-231 cell line using MTT assay revealing the dose-dependent cytotoxic effects. Mp-Au NPs dramatically increased the production of ROS, caused necrosis and nuclear damage and sensitised the mitochondrial membrane, which in turn set off the apoptotic cascade. The results highlight the potential of biowaste-derived Au NPs as promising candidates for biomedical applications, particularly in antioxidant therapy and cancer treatment.

Keywords: Biowaste, *Malus pumila*, Au NPs, DPPH assay, Cytotoxicity.

INTRODUCTION

The rapid advancement of nanotechnology has revolutionised various scientific domains including agriculture medicine and environmental sciences. Among the plethora of applications, the synthesis of nanoparticles has gained significant interest due to their unique physico-chemical properties and versatility in diverse fields [1]. Metal nanoparticles exhibit unique properties such as high surface area, optical tunability and enhanced reactivity, making them invaluable in various applications. Among the different metal nanoparticles, Au NPs have emerged as a versatile and highly effective platform for cancer diagnosis, therapy and drug delivery. The distinct electrical and optical characteristics of gold, high surface energy and excellent physical and chemical stability make it particularly desirable [2-5]. Their unique physico-chemical properties, biocompatibility and ease of functionalisation make them particularly advantageous for addressing the challenges associated with traditional cancer treatment methods [6,7].

Green synthesis or biosynthesis of nanoparticles employs natural biological entities such as plants, microorganisms and algae as reducing and stabilizing agents to synthesize nanoparticles. This approach is inspired by the natural ability of these biological systems to reduce metal ions into their nanoscale metallic forms [8]. Biowaste, including agricultural residues, fruit peels, vegetable scraps and food industry byproducts, is a rich source of bioactive compounds such as polyphenols, flavonoids, proteins and carbohydrates. These biomolecules serve as natural reducing and stabilizing agents during nanoparticle synthesis, eliminating the need for toxic chemicals and energy-intensive conventional methods. Owing to its affordability, sustainability and easy availability, biowaste-mediated synthesis

has emerged as a promising green approach for the production of metal nanoparticles [9]. In particular, fruit and vegetable peels, seeds, and other organic wastes have been widely utilized for the eco-friendly synthesis of silver and gold nanoparticles, with studies demonstrating their physico-chemical properties and biological activities [10-15]. The studies by Yuan *et al.* [16] and Madhumithra *et al.* [17] reported that the peels of *Citrus maxima* and shells of *Pistacia vera* effectively synthesised stable Au NPs. Similarly, *Garcinia mangostana* (mangosteen) peel extract has been used to produce Au NPs, with studies indicating that the phytochemicals present in the peel effectively mediate the reduction process [18]. These approaches not only provide a sustainable method for nanoparticles synthesis but also add value to agricultural waste materials.

The current work aimed to evaluate the aqueous extracts of seven selected fruit peels in order to synthesize biocompatible Au NPs. Furthermore, in order to better understand the cellular process of apoptosis in human breast epithelial adenocarcinoma (MDA-MB-231) cells as well as their antioxidant and cytotoxic properties, the stable biosynthesised Au NPs have been improved and reported.

EXPERIMENTAL

Preparation of biowaste extracts: The fruit peels of *Malus pumila* (apple) (Mp), *Musa acuminata* (banana) (Ma), *Vitis vinifera* (grapes) (Vv), *Citrus sinensis* (orange) (Cs), *Punica granatum* (pomegranate) (Pg), *Persea americana* (avocado) (Pa) and *Limonia acidissima* (wood apple) (La) separated from the pulp, cleaned and washed thoroughly with distilled water. The collected fruit peels were air-dried at room temperature for 3-5 days and ground into coarse powder. The powdered peel (5 g) was boiled in 100 mL of distilled water at 50-60 ºC for 30 min and kept in orbital shaker for overnight. After passing through Whatman No. 1 filter paper, the extract was kept for further use at 4 ºC.

Green synthesis of gold nanoparticles (Au NPs): For synthesis of gold nanoparticles, 1 mL of fruit peel extract was mixed with 9 mL of 1 mM $HAuCl_4$ solution and incubated at room temperature for 24 h. The colour change to pink/ruby red/purple indicated nanoparticles formation. A distinct colour change from a colourless solution to ruby red was observed, indicating the successful reduction of Au ions and the formation of Au NPs. A double beam UV-vis spectrophotometer operating in the wavelength range of 300-700 nm was used to assess the progress achieved by gold ion reduction using the peel extract to generate Au NPs. Furthermore, the Au NPs were observed and documented for any aggregation or precipitation. According to the observation, *M. pumila* (Mp) peel extract mediated synthesised gold nanoparticles (Mp-Au NPs) had a significant ruby red colour, indicating effective nanoparticles production and being employed for additional studies.

Optimisation of Mp-Au NPs: The optimisation of different parameters enhances the biocompatibility, stability and biomedical applicability of Au NPs, making them suitable for drug delivery. The following parameters were varied to optimize Mp-Au NPs like pH, temperature, precursor concentration and extract volume [19]. These parameters were optimised to achieve the maximum production and functionality of Mp-Au NPs. The reaction solution was optimised by exposing to different pH (5, 6, 7, 8 and 9) and various temperature conditions (15 ºC, 25 ºC, 35 ºC, 45 ºC and 55 ºC). Likewise, different concentration of $HAuCl_4$ (0.5, 1.0, 2.0, 3.0 and 4.0 mM) was added to reaction solution and held in a dark state for 24 h. Similarly, different volume of *M. pumila* extract (0.5 mL, 1 mL, 2 mL, 3 mL and 4 mL) based synthesis was checked. All the reactions were monitored by UV-Vis spectrophotometer in the wavelength range of 300-700 nm to confer the optimal conditions for stable Mp-Au NPs synthesis.

Stability analysis of Mp-Au NPs: The absorbance in the 300–700 nm range was measured at regular intervals (24 h, 48 h, 10 days, 20 days, 30 days and 45 days) to evaluate the stability of the biosynthesized Mp-Au NPs under optimized conditions.

Antioxidant activity: The DPPH free radical scavenging experiment was used to assess the antioxidant activity of the biosynthesised Mp-Au NPs using the procedure outlined by Kowsalya *et al.* [20]. DPPH solution (4 mM) was prepared in methanol and stored in the dark at room temperature. Various concentrations of the biosynthesised Mp-Au NPs (20, 40, 60, 80, 100 µg/mL) were mixed with 2 mL of DPPH solution and incubated in the dark for 20 min at 37 ºC. The absorbance of the reaction mixture was measured at 517 nm using a UV-Vis spectrophotometer. The following formula was used to determine the percentage of DPPH radical scavenging activity:

$$\text{Radical scavenging activity (\%)} = \frac{\text{Abs}_{\text{control}} - \text{Abs}_{\text{sample}}}{\text{Abs}_{\text{control}}} \times 100$$

Qualitative phytochemical analysis: The peel extract of *M. pumila* was subjected to the qualitative phytochemical screening to identify the presence of bioactive compounds, including alkaloids, carbohydrates, glycosides, saponins, amino acids, proteins, phenolic compounds, flavonoids, terpenoids, and steroids. The analysis was performed using standard methods described by Iqbal *et al.* [21].

Characterisation: The size distribution and morphological features of Mp-Au NPs were evaluated using a Transmission Electron Microscopy (TEM) set at 200 kV. Using energy dispersive X-ray (EDX) analysis and selected area electron diffraction (SAED), the existence of the distinct elemental composition and crystalline structure data was confirmed. The crystalline structures and phase purity of synthesised Mp-Au NPs were examined using X-ray diffraction (XRD) experiments using Cu*K*α radiation (λ = 1.5406 Å). To determine the functional groups in charge of the nanoparticles production, Fourier-transform infrared spectroscopy (FTIR) was used for Mp-Au NPs and apple peel extract in the 4000-400 cm^{-1} range.

***In vitro* cytotoxicity assessment:** The cytotoxic effect of biosynthesized Mp-Au NPs against MDA-MB-231 and 3T3/NIH cell lines was evaluated using the MTT assay [22]. The human breast adenocarcinoma epithelial cell line (MDA-MB-231) and normal fibroblast cell line (3T3/NIH) were obtained from the National Centre for Cell Sciences (NCCS), Pune, India. Cells were maintained in Dulbecco's Modified Eagle Medium (DMEM) supplemented with 10% (v/v) heat-inactivated fetal bovine serum (FBS), 100 U/mL penicillin,

and 100 μg/mL streptomycin and incubated at 37 ºC in a humidified atmosphere containing 5% CO_2. The cells were seeded into 96-well microtitre plates at a density of 1×10^4 cells/well and incubated for 48 h until 70-80% confluence was achieved. The cells were then treated with different concentrations of Mp-Au NPs (20, 40, 60, 80 and 100 μg/mL) and incubated for an additional 24 h. Morphological changes in treated and untreated (control) cells were observed and photographed using a digital inverted microscope at 20× magnification. After treatment, the cells were washed with phosphate buffered saline (PBS, pH 7.4), followed by the addition of 20 μL MTT solution (5 mg/mL in PBS) to each well. The plates were incubated in the dark for 4 h at 37 ºC. The resulting formazan crystals were dissolved in 100 μL DMSO and the absorbance was measured at 570 nm using a spectrophotometer. The following equation was used to determine the percentage of cell viability:

$$\text{Cell viability (\%)} = \frac{\text{Absorbance of sample}}{\text{Absorbance of control}} \times 100$$

Apoptotic morphological detection by AO/PI dual staining: The apoptosis and necrosis morphological changes induced by Mp-Au NPs were assessed using the acridine orange/propidium iodide (AO/PI) dual staining assay, following the method described by Uzma *et al*. [23] with slight modifications. The MDA-MB-231 cancer cells was seeded in 6-well plates at a density of 1×10^5 cells per well and incubated at 37 ºC with 5% CO_2 for 24 h to allow cell attachment. After incubation, the cells were treated with IC_{50} concentration of Mp-Au NPs and incubated for 24 h. The untreated cells served as the control group. Following treatment, the cells were washed with phosphate-buffered saline (PBS) and stained with 10 μL of AO/PI staining solution (100 μg/mL AO and 100 μg/mL PI in PBS). The cells were then incubated in dark for 5 min at room temperature. The stained cells were observed under a fluorescence microscope (Invitrogen EVOS FL Cell Imaging; 40× magnification).

Nuclear morphology analysis by DAPI staining: Using the DAPI (40-60-diamidino-2-phenylindole) staining method, the nuclear morphological modifications (condensed chromatin and fragmented nuclei) in MDA-MB-231 cells treated with Mp-Au NPs were identified [24]. The fixed cells were stained with DAPI dye, which binds strongly to DNA sequences rich in adenine and thymine. In six-well plate, 1×10^5 cells per well were cultured and treated with IC_{50} concentration of Mp-Au NPs for 24 h. Following incubation, the cells were rinsed with PBS, fixed for 10 min with 3% paraformaldehyde (50 μL) and permeabilised for 10 min at room temperature using 0.2% Triton X-100 (50 μL). Following 5 min of staining with 10 μL of DAPI stain (0.5 μg/mL), the cells were examined under a fluorescence microscope.

Reactive oxygen species (ROS) analysis by DCFH-DA staining: The intracellular ROS levels were determined using 2′,7′-dichlorodihydrofluorescein diacetate (DCFH-DA), a non-fluorescent compound that is converted to a highly fluorescent compound upon oxidation by intracellular ROS [25]. The MDA-MB-231 cells were seeded in a six-well plate at 1×10^5 cells/well and incubated for 24 h at 37 ºC in a 5% CO_2 atmosphere. The cells were treated with IC_{50} concentrations of biosynthesised Mp-Au NPs for 24 h. Untreated cells were used as the control. Following treatment, the cells were rinsed with PBS and left to incubate for 30 min at 37 ºC in the dark with 10 μM DCFH-DA dissolved in DMSO. Cells were rinsed with PBS to get rid of extra colour after incubation. Using a fluorescent microscope, the DCF formation inside the cells was photographed.

Assessment of mitochondrial membrane potential (Δψm): Rhodamine 123 staining, a cationic dye that builds up in mitochondria and shows a potential-dependent fluorescence shift from red to green, was used to measure the mitochondrial membrane potential (Δψm). An early indicator of apoptosis, loss of Δψm, was assessed using the methodology of Jiang *et al*. [26]. After being seeded at a density of 1×10^5 cells/well in a six-well plate, the MDA-MB-231 cells were incubated for 24 h. The cells were treated with IC_{50} concentrations of biosynthesised Mp-Au NPs for 24 h. The control group consisted of untreated cells. Following treatment, the cells were rinsed with PBS and left in the dark at 37 ºC for 30 min with 10 μM rhodamine 123 dye. In order to get remove of excess dye, the cells were rinsed with PBS after incubation. Using a fluorescence microscope, the morphological variations and membrane permeability were recorded.

DNA fragmentation: The DNA fragmentation assay method was used to evaluate the apoptosis by detecting internucleosomal DNA cleavage in agarose gel electrophoresis [27]. Briefly, MDA-MB-231 cells were cultured in 25 cm^2 cell culture flasks for 48 h and then subjected to the IC_{50} concentration of Mp-Au NPs for 24 h. Centrifugation was then used to extract the cells after they had been gently scraped. After being reconstituted in 0.5 mL of lysis buffer (10 mM Tris-HCl, 0.5 mM EDTA (pH 8.0), 2% SDS and 1 mM NaCl), the cells were incubated for 15 min at 37 ºC. To denature the protein content and purify the DNA, proteinase K (20 mg/mL) was added. After 45 min of incubation at 50 ºC, the mixture was extracted using an equivalent volume of phenol:chloroform: isoamyl alcohol (25:24:1) solution. After treating the mixture with 3M sodium acetate (100 μL), the DNA was precipitated by adding ice-cold 70% ethanol (200 μL). After the DNA was electrophoretically examined in 1% agarose gels containing 0.1 μg/mL ethidium bromide, the picture was captured using a gel documentation system.

Statistical analysis: Every experiment was carried out in triplicate and the mean ± standard deviation (SD) was used to express the data. Microsoft Excel 2013 was used to create the graphical representation.

RESULTS AND DISCUSSION

Biosynthesis screening of Au NPs: The fruit peel extract of *M. pumila*, *M. acuminata*, *V. vinifera*, *C. sinensis*, *P. granatum*, *P. americana* and *L. acidissima* were tested for synthesis of Au NPs. The peels of *M. pumila*, *V. vinifera*, *C. sinensis*, *P. americana* and *L. acidissima* resulted in a rapid colour change from white/yellow to pink or ruby red or purple (Fig. 1), suggesting successful reduction of Au^{3+} ions to Au^0 nanoparticles.

Utilizing the biowaste not only aligns with sustainable practices but also offers a valuable method for nanoparticles

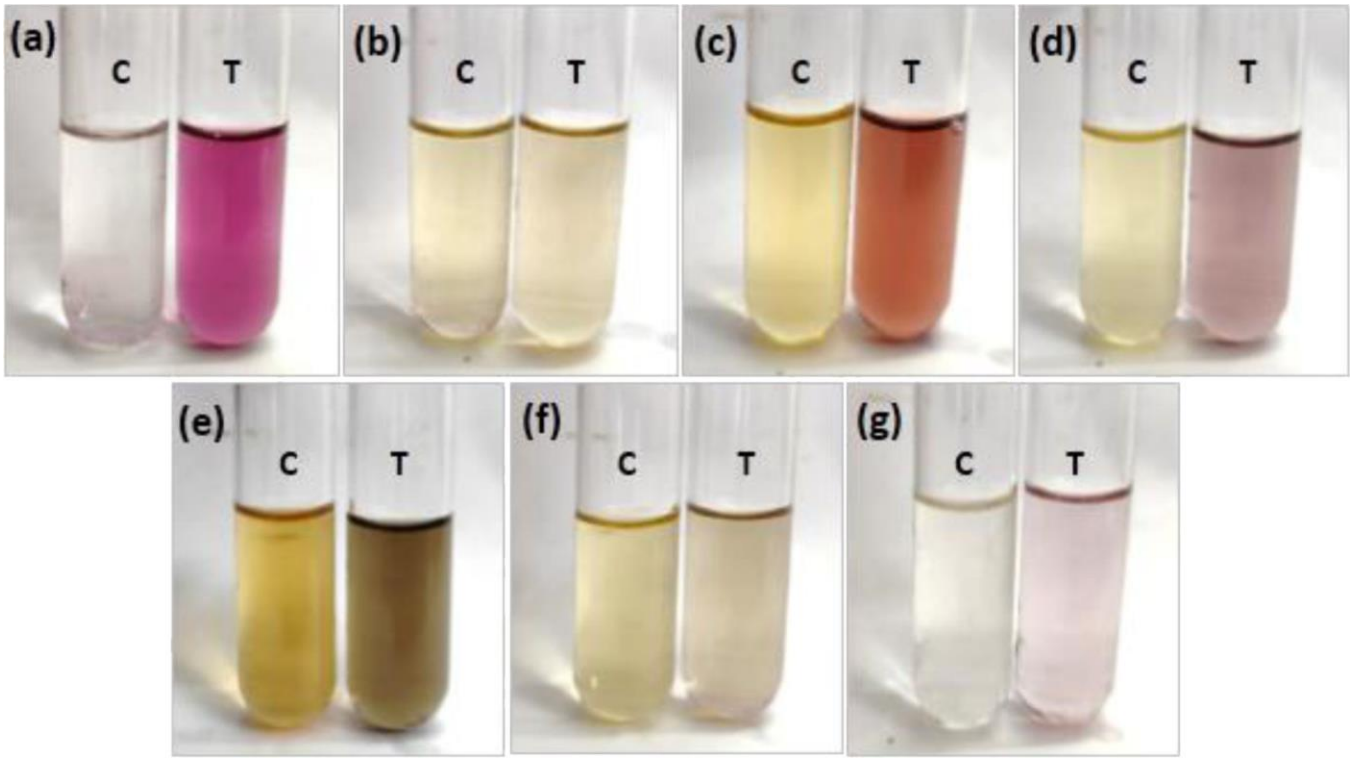

Fig. 1. Screening of Au NPs synthesis using different peel extracts. (a) *M. pumila*, (b) *M. acuminata*, (c) *V. vinifera*, (d) *C. sinensis*, (e) *P. granatum*, (f) *P. americana* and (g) *L. acidissima* C, control and T, test

synthesis. In addition, the formation of Au NPs was further confirmed by the surface plasmon resonance (SPR) peak in the range of 500-550 nm examined using UV-Vis spectroscopy. Among the tested samples, Mp-Au NPs exhibited the strongest and most stable peak and strong peak at 535 nm, indicating well-formed and monodispersed nanoparticles (Fig. 2). The Vv-Au NPs (moderate peak at 545 nm), Cs-Au NPs (shallow peak at 525 nm), Pa-Au NPs (low peak at 550 nm) and La-Au NPs (shallow peak at 510 nm) also showed SPR peaks within the expected range (Fig. 2), but with slightly lower intensity compared to Mp-Au NPs.

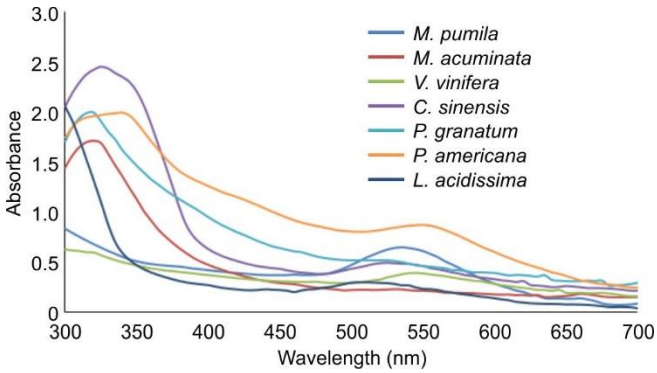

Fig. 2. UV-vis spectroscopic analyses

Yuan *et al*. [16] reported the synthesis of Au NPs using *Citrus maxima* peel extract with a characteristic peak at 540 nm. The distinctive absorption peaks which are stronger and more symmetric at lower concentrations of $HAuCl_4$, indicates that the produced Au NPs were monodispersed in the solution [28,29]. However, *M. acuminata* and *P. granatum* peels did not exhibited a significant colour change and SPR peaks, indicating unsuccessful nanoparticles formation which may be attributed to a lower concentration of bioactive compounds or the presence of inhibitory components that interfere with Au ions reduction. The other peel extracts (except *M. pumila)* fail to achieve stable and efficient result because the biomolecules do not provide consistent reducing agents. Therefore, *M. pumila* peel extract was selected to obtain the gold nanoparticles for the further detailed investigation.

Optimisation of different parameters for Mp-Au NPs synthesis: The reaction conditions play a crucial role in maximizing the production, stability and size of biosynthesised Au NPs [30]. In Fig. 3a, Mp-Au NPs synthesis was most effective at neutral pH 7, where a ruby red colour and a distinct SPR peak at 535 nm were observed. At pH 6 and pH 8, the synthesis yielded pink and purple colours, respectively, accompanied by mild SPR peaks at 520 nm and 550 nm, indicating less efficient nanoparticle formation. The absence of characteristic colour changes and SPR peaks at pH 5 and pH 9 indicates that Au NP synthesis was inhibited, possibly due to the unfavorable effects of extreme pH conditions on nanoparticle formation. In contrast, pH 7 promoted the formation of isotropic Au NPs and was therefore considered the optimal pH for the synthesis process [31]. This observation aligns with earlier studies by Singh *et al*. [32] and Kowsalya *et al*. [20], who also identified pH 7 as optimal for Au NPs formation.

Fig. 3b illustrated that the synthesis of Au NPs was most efficient at 35 ºC, as evidenced by a distinct SPR peak at 535 nm, indicating the formation of small-sized nanoparticles. At lower temperatures of 15 ºC and 25 ºC, the synthesis yielded

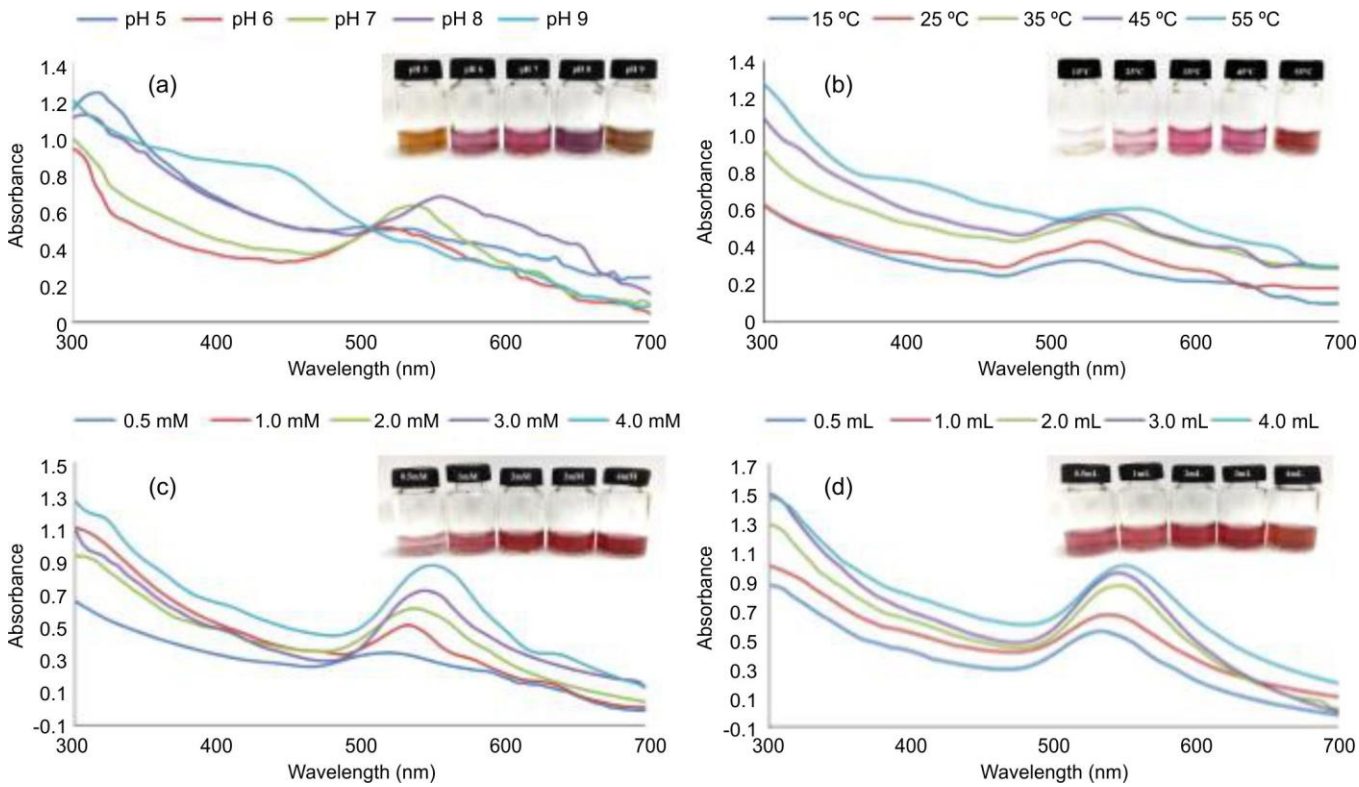

Fig. 3. Synthesis and UV-vis spectra of synthesised Mp-Au NPs in varying reaction parameters. (a) different concentrations of $HAuCl_4$, (b) different volume of *M. pumila* extract, (c) different pH and (d) different temperatures

faint colour changes and shallow SPR peaks at 515 nm and 525 nm, respectively, suggesting a reduced number of nanoparticles. Conversely, higher temperatures (45 ºC and 55 ºC) resulted in a red shift and broadening of the SPR peaks (540 nm and 560 nm), indicative of larger nanoparticle sizes. These findings are consistent with previous studies [20,24], which reported that temperature 37 ºC is favourable for the synthesis of Au NPs. Similarly, other research has demonstrated that higher temperatures can lead to the formation of larger nanoparticles, as observed by a red shift and broadening of the SPR peak [33]. Therefore, 35 ºC was considered as the optimal temperature for Au NPs synthesis, promoting the formation of small-sized nanoparticles with a distinct SPR peak.

The concentration of gold salt ($HAuCl_4$) plays a crucial role in the synthesis of Au NPs. UV-Vis analysis of different $HAuCl_4$ concentrations (0.5-4.0 mM) showed that increasing the concentration enhanced the absorbance intensity, indicating higher nanoparticle formation (Fig. 3c). Among the tested concentrations, 1 mM $HAuCl_4$ was found to be optimal for the synthesis of Au NPs using *M. pumila* peel extract, as evidenced by the formation of a ruby red colour and an SPR peak at 535 nm. Similar findings were reported by Mansoori *et al*. [34] for *Melissa officinalis*-mediated Au NPs synthesis.

The effect of *M. pumila* peel extract volume on Mp-Au NPs formation was also evaluated using UV-Vis spectroscopy (Fig. 3d). At 0.5 mL extract, an SPR peak at 530 nm indicated the initiation of nanoparticle formation, accompanied by a colour change from yellow to pale ruby pink. An 1 mL of extract volume produced stable and monodispersed Mp-Au NPs with an SPR peak at 535 nm. However, extract volumes above 2 mL resulted in increased absorbance intensity, peak broadening and a slight redshift, suggesting nanoparticle aggregation due to excess biomolecules interfering with uniform nanoparticle formation [35]. These observations support the report by Sharma *et al*. [36], which highlighted the importance of the extract-to-metal precursor ratio in nanoparticle synthesis.

Stability analysis of Mp-Au NPs: The stability of Au NPs synthesized using *M. pumila* extract was evaluated over a 45 day period using UV-Vis spectroscopy (Fig. 4). The absorbance peak remained stable from 24 h to 45 days, with no significant changes in colour or evidence of nanoparticle aggregation. These results indicate the excellent stability of the synthesized Au NPs throughout the study period [37].

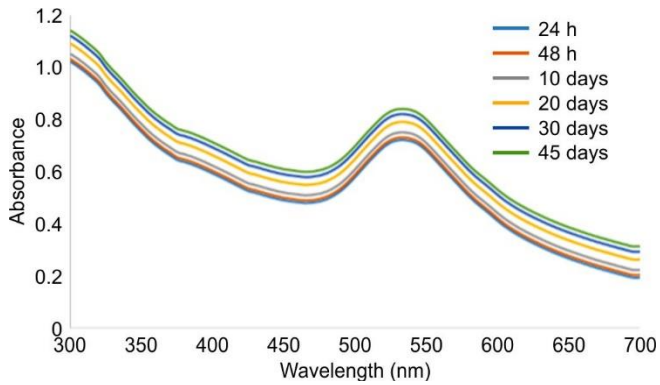

Fig. 4. UV-vis spectra depicting stability of Mp-Au NPs at different time periods

Antioxidant activity: Mp-Au NPs exhibited significant DPPH free radical scavenging activity, as indicated by the

colour change from purple DPPH radicals to yellow diphenyl picrylhydrazine. The nanoparticles showed a strong dose-dependent antioxidant effect (Fig. 5), achieving 79.45% DPPH radical scavenging at 100 µg/mL. Similar findings were reported by Li *et al*. [38], who demonstrated that flavonol-Au NPs possessed higher antioxidant activity than flavonol or Au NPs alone.

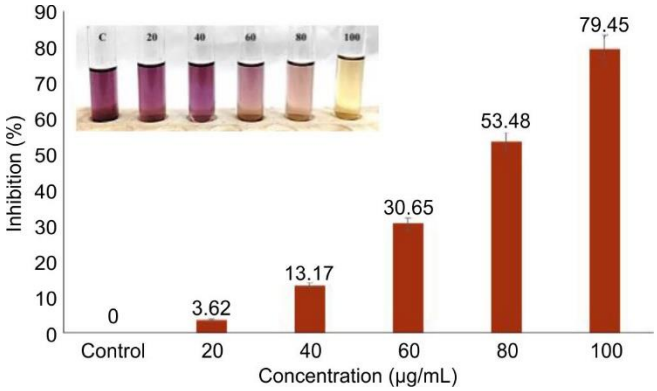

Fig. 5. Antioxidant activity of Mp-Au NPs. Data are means ± SE of three observations with different letters indicating statistically significant differences ($p < 0.05$)

Qualitative phytochemical studies: Phytochemical analysis of the *M. pumila* peel extract revealed the presence of bioactive compounds such as alkaloids, carbohydrates, glycosides, saponins, phenolic compounds, and flavonoids, which play an important role in the synthesis of Mp-Au NPs. These biomolecules act as reducing and stabilizing agents by facilitating the conversion of Au^{3+} ions to Au^0 and preventing nanoparticle aggregation. The findings are consistent with previous reports highlighting the role of polyphenols and flavonoids in gold nanoparticle synthesis [39]. The abundance of these bioactive compounds in apple peels further suggests that fruit peel waste can serve as an effective and sustainable resource for green nanotechnology applications [40].

Characterisation of Mp-Au NPs

Transmission electron microscope (TEM): The TEM was used to examine the size and shape of the synthesised Mp-Au NPs, as shown in Fig. 6a-b. The Mp-Au NPs are evenly distributed and the *M. pumila* matrix envelops them, suggesting that the matrix serves as a capping agent to prevent aggregation. The obtained Au NPs have an average size of 32.96 ± 5.25 nm and are primarily spherical, with some hexagonal and triangular shapes. Similar results were found for Au NPs made with pomegranate peel extract, which showed a range of geometries, including triangular and spherical forms, with an average size of about 20.65 nm and diameters ranging from 6.75 to 57.91 nm [41]. According to a study by Lee *et al.* [18], Au NPs made from the peel of the *Garcinia mangostana* fruit were widely distributed, primarily subspheroidal and ranged in size from 8 to 25 nm (majority were about 15 nm).

SAED pattern: The observed concentric rings correspond to the (111), (200), (220) and (311) planes of face-centered cubic (FCC) crystalline gold (Fig. 6c). These diffraction patterns are consistent with the standard JCPDS data for gold

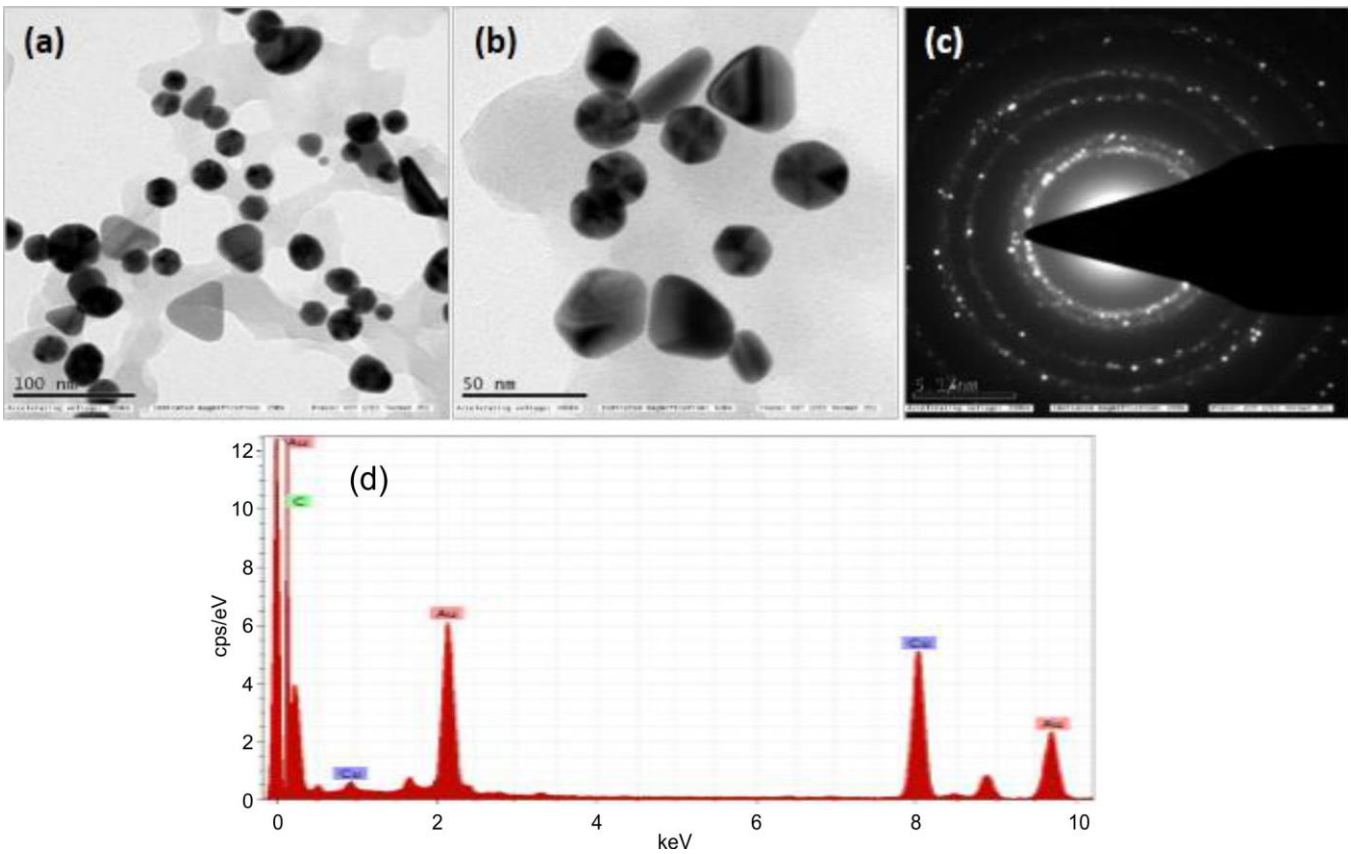

Fig. 6. Characterisation of Mp-Au NPs. (a & b) HR-TEM micrograph; (c) SAED pattern and (d) EDX spectrum

(No. 04-0784), confirming the crystalline nature of the synthesized nanoparticles. The sharp and intense diffraction rings further indicate the formation of well-ordered crystalline Au NPs through effective reduction and nucleation of gold ions. Similar FCC diffraction patterns have also been reported for Au NPs synthesized using banana peel extract by Jain & Mehata [42] and *Vitis vinifera* peel extract by Rastogi *et al.* [43].

EDAX studies: The EDAX spectrum of synthesised Mp-Au NPs showed a strong gold signal at 2.2 keV, confirming the presence of elemental gold (Fig. 6d). Additional peaks at 8.4, 9.6 and 11.4 keV further verified the metallic nature of Au NPs. Signals for carbon and oxygen indicated the presence of phytochemical residues from *M. pumila* peel extract, suggesting their role in reduction and stabilisation of nanoparticles. These organic molecules likely remained adsorbed on the nanoparticle surface as capping agents. The dominance of gold peaks with minor impurity signals confirmed successful synthesis and purity, consistent with previous green synthesis studies, as described by Yuan *et al*. [16] and Zuorro *et al*. [44].

XRD studies: The crystalline nature of the Mp-Au NPs was characterised by XRD illustrated in Fig. 7. The diffraction peaks at (2θ) 38.08º, 44.26º, 64.46º and 77.40º were assigned to (111), (200), (220) and (311) planes of the face-centered cubic (fcc) lattice of gold (JCPDS no. 04-0784). The results demonstrated that the biosynthesised Au NPs were crystalline in nature. Au NPs synthesised using pineapple and passion fruit peel extracts exhibited XRD patterns with peaks at 38.1º, 44.3º, 64.5º and 77.4º, corresponding to the (111), (200), (220) and (311) planes of fcc gold [45]. These findings are consistent with the SAED pattern data, which also confirmed the crystalline nature of the particles.

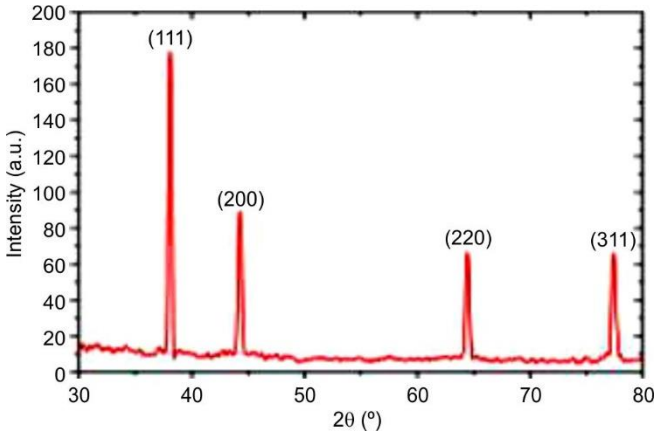

Fig. 7. XRD pattern of Mp-Au NPs

FTIR studies: FTIR analysis revealed significant changes in the peak positions and intensities after nanoparticle synthesis, indicating the involvement of bioactive compounds from *M. pumila* peel extract in the formation of Mp-Au NPs. The extract spectrum showed characteristic absorption bands at 3280, 2920, 1610 and 1025 cm^{-1}, corresponding to O–H stretching, aliphatic C–H stretching, amide-I (C=O) stretching, and C–O–C vibrations, respectively. Peaks between 1400-1450 cm^{-1} were attributed to C–H bending vibrations, while bands near 1100-1020 cm^{-1} indicated alcohol or ether groups (Fig. 8a).

In the Mp-Au NPs spectrum (Fig. 8b), similar peaks were observed with slight shifts, confirming interactions between functional groups and Au ions. The shift of the hydroxyl peak from 3280 to 3265 cm^{-1} suggested hydrogen bonding or metal coordination during nanoparticle synthesis, while broadening of the amide-I band indicated possible involvement of proteins in the nanoparticle stabilization. Polyphenols, flavonoids and proteins present in the apple peel extract likely contributed to the reduction of Au^{3+} to Au^0 and stabilization of the nanoparticles through capping. Phenolic compounds may facilitate metal ion reduction *via* oxidation of aldehydes to carboxylic acids.

***In vitro* cytotoxicity assessment of Au NPs:** Mp-Au NPs were tested for cytotoxicity in 3T3 and MDA-MB-231 cell lines using a range of doses, from 20 µg/mL to 100 µg/mL. Following a 24 h exposure period, 3T3 cells exhibited little morphological alterations (Fig. 9), with 91.79% cell viability at the maximum dosage of 100 µg/mL. However, starting at lower concentrations, Mp-Au NPs changed the shape of MDA-MB-231 cells (Fig. 10). They also demonstrated a considerable dose-dependent suppression of MDA-MB-231 cell growth, with an IC_{50} value of 74.74 µg/mL (Fig. 11). According to the study, Mp-Au NPs interfered with cellular reproduction, metabolic activity, membrane integrity and membrane potential [46].

Apoptotic morphological detection by AO/PI dual staining: Fluorescence microscopy identified different cell populations based on nuclear staining patterns. Viable cells exhibited intact green nuclei, while early apoptotic cells showed

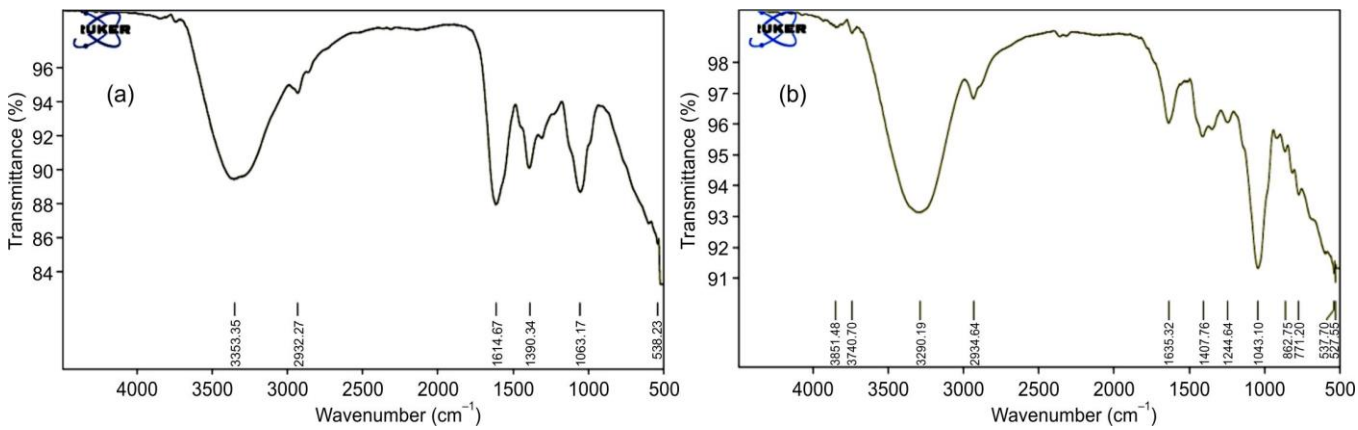

Fig. 8. FTIR spectra. (a) *M. pumila* extract and (b) synthesised Mp-Au NPs

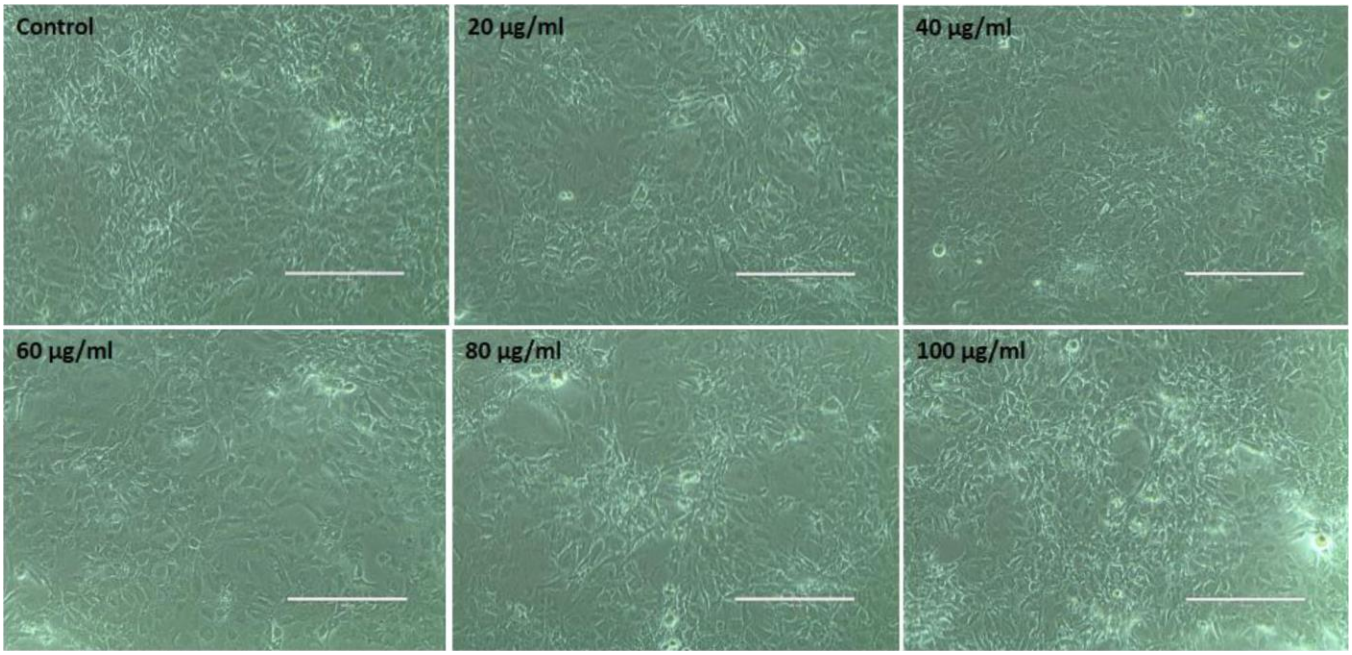

Fig. 9. Cytotoxic activity of different concentrations of Mp-Au NPs against 3T3 cells

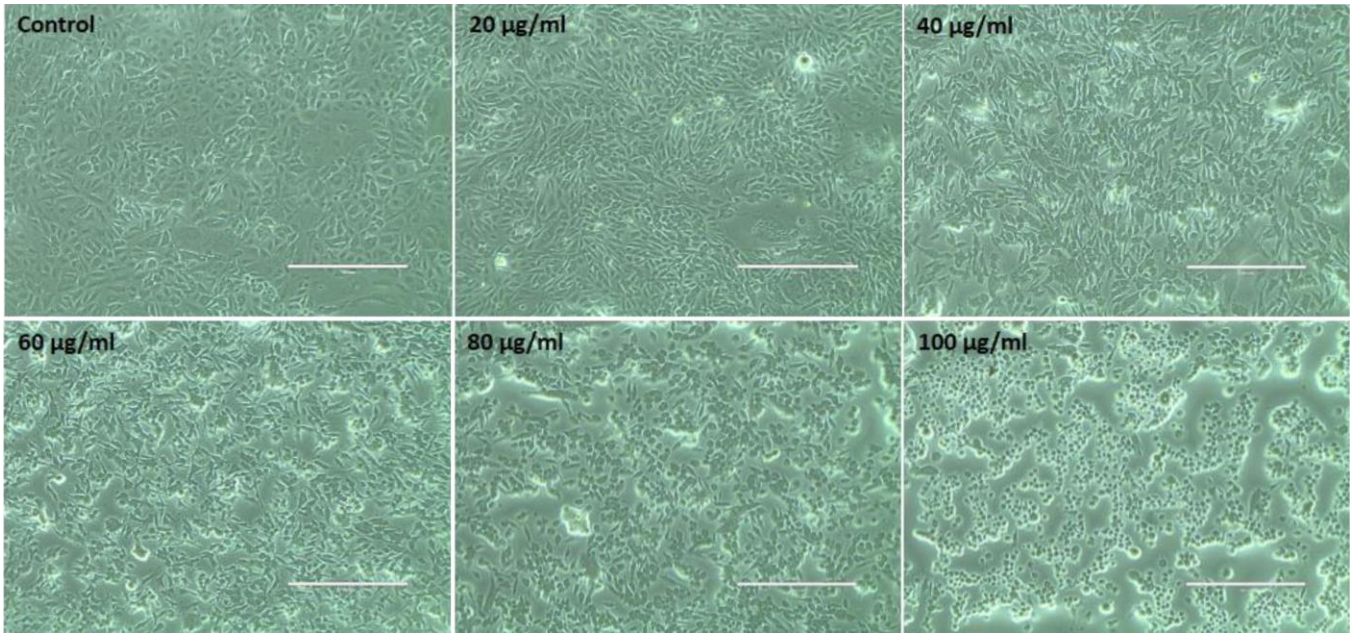

Fig. 10. Cytotoxic activity of different concentrations of Mp-Au NPs against MDA-MB-231 cells

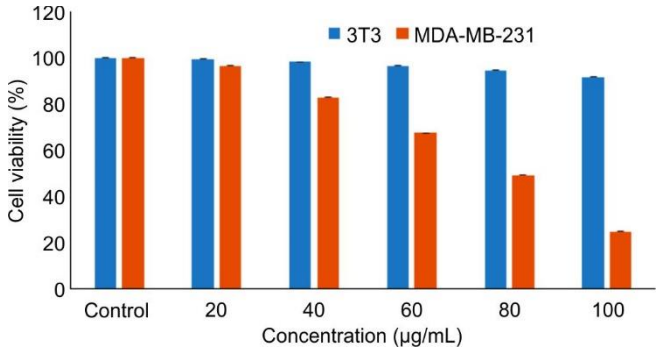

Fig. 11. Cell viability (%) by MTT assay (data represents means ± SE of three replicates)

greenish-yellow nuclei. Late apoptotic cells displayed orange or red fluorescence due to PI uptake and nuclear fragmentation, whereas necrotic cells exhibited intense red fluorescence with complete nuclear disintegration. AO/PI dual staining confirmed that the synthesized Mp-Au NPs induced apoptosis in MDA-MB-231 cells (Fig. 12a), as evidenced by nuclear condensation, fragmentation and membrane blebbing, which are the characteristic features of programmed cell death. The presence of both early and late apoptotic cells indicates a gradual progression of apoptosis rather than immediate necrosis [47]. This observation is consistent with established apoptotic pathways involving chromatin condensation, DNA fragmentation and membrane blebbing prior to necrosis [48].

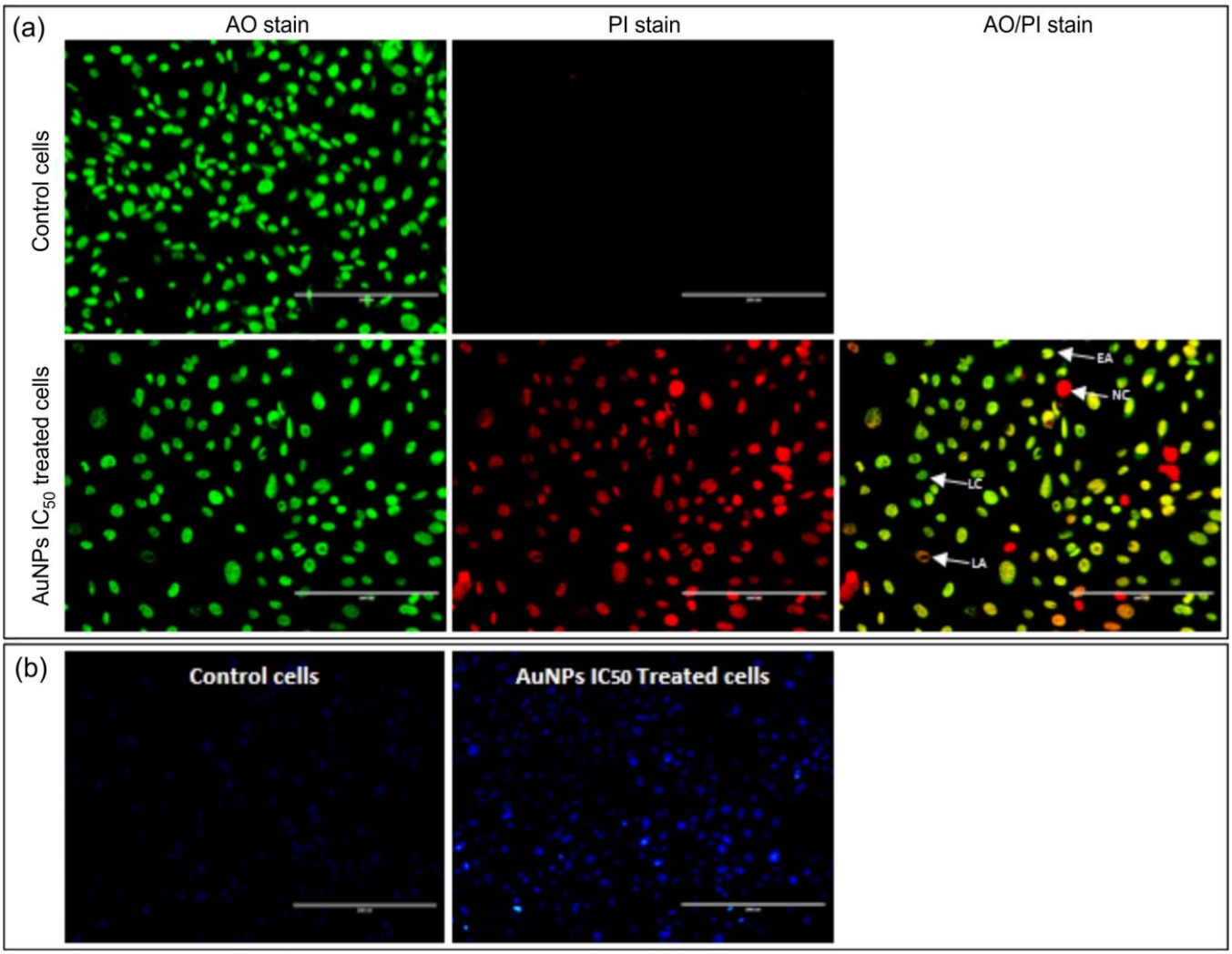

Fig. 12. Fluorescence microscopy images of Mp-Au NPs treated MDA-MB-231 cells. (a) AO/PI dual staining, (b) DAPI staining

Nuclear morphology analysis by DAPI staining: DAPI-stained MDA-MB-231 cells treated with Mp-Au NPs showed significant morphological changes consistent with apoptosis. These included chromatin condensation, nuclear fragmentation and bright blue fluorescence indicating apoptotic nuclei. Along with a loss of cell structure displaying blue fluorescence with white condensed patches, the number of nuclear alterations was also observed. These morphological characteristics, in particular nuclear fragmentation and chromatin condensation, are suggestive of late-stage apoptosis and support the results of DNA fragmentation and other apoptosis tests (Fig. 12b). In contrast, control (untreated cells) displayed uniform, round nuclei with no signs of condensation or fragmentation. These observations align with studies by Rizwan *et al*. [49] and Jung *et al*. [50], where DAPI staining effectively revealed apoptotic changes in cancer cells treated with plant-derived or metallic nanoparticles.

Intracellular ROS generation by DCFH-DA staining: The DCFH-DA assay uses the formation of a fluorescent product (DCF) following oxidation by free radicals to quantify intracellular ROS generation. Compared to the control group, treatment with Mp-Au NPs (IC_{50}: 74.74 µg/mL) resulted in a significant increase in intracellular ROS production (Fig. 13a). Cells treated with Mp-Au NPs exhibited stronger green fluorescence signals, indicating elevated oxidative stress. The enhanced ROS generation is likely due to the cellular internalization of Au NPs and their interaction with intracellular organelles, particularly mitochondria. Increased oxidative stress can trigger apoptosis in cancer cells through damage to DNA, proteins, and lipids. These findings highlight the potential of biogenic Au NPs in oxidative stress-mediated anticancer therapy. Similar results have been reported for polyphenol-capped Au NPs, which induced cancer cell cytotoxicity through ROS generation *via* redox cycling [51].

Assessment of mitochondrial membrane potential (Δψm) by Rh-123 staining: Mitochondrial membrane depolarisation is a hallmark of apoptosis and plays a critical role in cell death pathway [47]. The mitochondrial membrane potential (Δψm) was evaluated in MDA-MB-231 cells treated with Mp-Au NPs (Fig. 13b). Rh-123 staining revealed a shift in fluorescence from red (aggregated rhodamine 123 in intact mitochondria) to green (monomeric rhodamine 123 in depolarised mitochondria) in IC_{50} concentration treated cells. The Mp-Au NPs treated cells showed a significant decreased green fluorescence, suggesting mitochondrial depolarisation and early apoptosis. The observed shift in fluorescence intensity

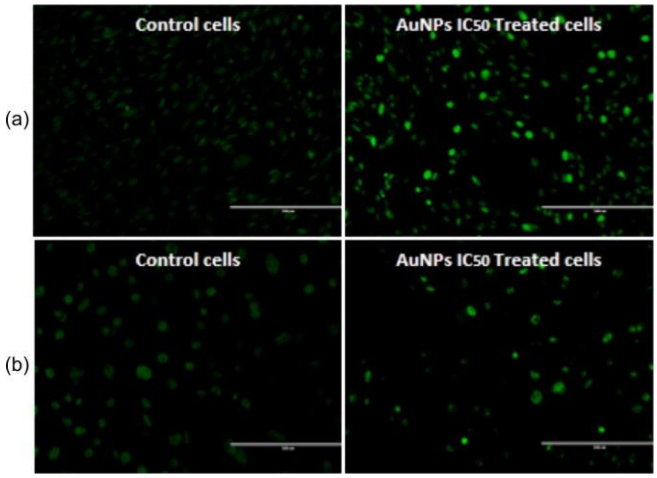

Fig. 13. Mp-Au NPs induced apoptotic-associated intrinsic changes in MDA-MB-231 cells. (a) DCFH-DA staining and (b) Rh-123 staining

suggests that Mp-Au NPs induce apoptosis by disrupting mitochondrial integrity, leading to cytochrome c release and caspase activation. These findings align with previous studies where metal-based nanoparticles exhibited pro-apoptotic activity *via* mitochondrial dysfunction [48]. Furthermore, the selective effect of nanoparticles on MDA-MB-231 cells, with minimal toxicity to 3T3 cells, suggests their potential biocompatibility and therapeutic application in cancer treatment. This is consistent with research by Lee *et al*. [52], which used JC-1 labelling to show that green-synthesised nanoparticles specifically impair mitochondrial activity in malignant cells while preserving normal cells.

DNA fragmentation: DNA fragmentation was evident in MDA-MB-231 cells treated with Mp-Au NPs, particularly at IC_{50} concentration, as observed by the appearance of distinct DNA ladders on the agarose gel (Fig. 14). The genomic DNA of untreated control cells was found to be intact and unfragmented, suggesting that the nanoparticles had a specific cytotoxic effect on cancer cells. The induction of apoptosis through the intrinsic mechanism is confirmed by the formation of a DNA ladder pattern in treated MDA-MB-231 cells. The fragmentation of DNA into oligonucleosomal units is a hallmark of late-stage apoptosis. These results agree with the previous reports, where plant-mediated nanoparticles induced apoptosis through mitochondrial pathways leading to DNA cleavage [53,54]. The study validates the apoptotic potential of biosynthesised Au NPs and supports their application in targeted cancer therapy.

Conclusion

The green synthesis of Au NPs utilizing various fruit peel extracts as biowaste was used in this study as an economical and environmentally beneficial method. Synthesised Au NPs mediated by *M. pumila* peel extract shown good stability and the capacity to operate as a potent antioxidant. The possible biocompatibility of Mp-Au NPs with healthy cells offers a promising future for their application in biomedical research. It was found that Mp-Au NPs inhibited the growth of MDA-MB-231 cells and revealed the anticancer activity in a dose-dependent manner. Several fluorescence staining methods were employed to verify that Mp-Au NPs successfully stimulated DNA damage in breast cancer cells, resulting in apoptosis and necrosis. The physico-chemical and anti-carcinogenic properties of Mp-Au NPs indicate their significant cytotoxic potential against breast adenocarcinoma cells. However, further *in vivo* studies are required to validate the therapeutic efficacy and safety of Mp-Au NPs observed in the present study.

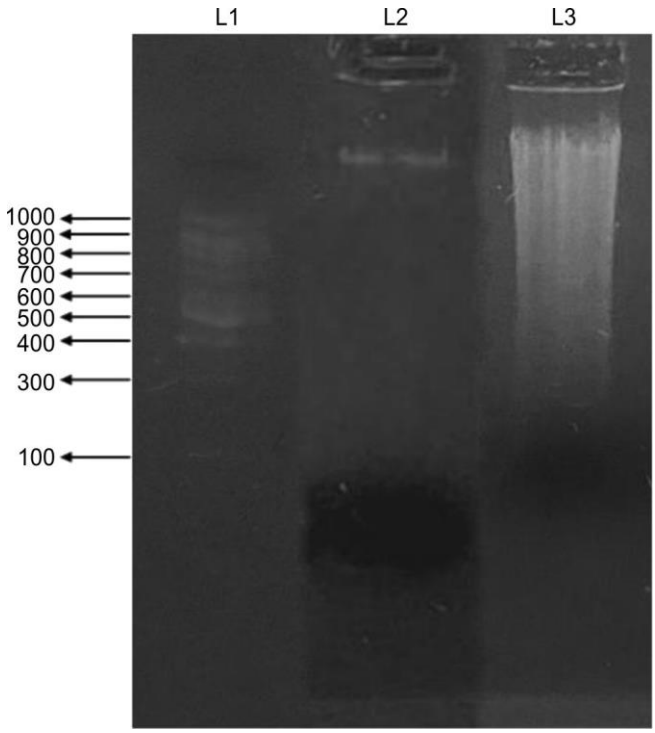

Fig. 14. DNA fragmentation assay in MDA-MB-231 cells. L1 - ladder; L2 - control DNA; L3 - IC_{50} treated DNA

CONFLICT OF INTEREST

The authors declare that there is no conflict of interests regarding the publication of this article.

DECLARATION OF AI-ASSISTED TECHNOLOGIES

During the preparation of this manuscript, the authors used an AI-assisted tool(s) to improve the language. The authors reviewed and edited the content and take full responsibility for the published work.

REFERENCES

1. S. Falsini and U. Bardi, *Green Chem.*, **20**, 3897 (2018); https://doi.org/10.1039/C8GC01248B
2. S. Alex and A. Tiwari, *J. Nanosci. Nanotechnol.*, **15**, 1869 (2015); https://doi.org/10.1166/jnn.2015.9718
3. R. Chen, F. Chen, M. Sun, R. Zhang, S. Wu and C. Meng, *Inorganic and Nano-Metal Chemistry*, **52**, 1345 (2022); https://doi.org/10.1080/24701556.2021.1952242
4. M. Aili, K. Zhou, J. Zhan, H. Zheng and F. Luo, *J. Mater. Chem. B*, **11**, 8605 (2023); https://doi.org/10.1039/D3TB01023F
5. M. Sharifi-Rad, Y. Kishore Mohanta, P. Pohl, D. Nayak and M. Messaoudi, *J. Photochem. Photobiol. Chem.*, **446**, 115150 (2023); https://doi.org/10.1016/j.jphotochem.2023.115150
6. V. Budhwar, *J. Chem. Pharm. Res.*, **8**, 259 (2016).

7. H. Singh, M.F. Desimone, S. Pandya, S. Jasani, N. George, M. Adnan, A. Aldarhami, A.S. Bazaid and S.A. Alderhami, *Int. J. Nanomedicine*, **18**, 4727 (2023); https://doi.org/10.2147/IJN.S419369
8. M.S. Samuel, M. Ravikumar, E. Selvarajan, H. Patel, P.S. Chander, A. John, J. Soundarya, S. Vuppala, R. Balaji and N. Chandrasekar, *Catalysts*, **12**, (2022); https://doi.org/10.3390/catal12050459
9. K. Bhardwaj and A.K. Singh, *Chem. Eng. J. Adv.*, **16**, 100536 (2023); https://doi.org/10.1016/j.ceja.2023.100536
10. G. Gnanajobitha, K. Paulkumar, M. Vanaja, S. Rajeshkumar, C. Malarkodi, G. Annadurai and C. Kannan., *J. Nanostructure Chem.*, **3**, 67 (2013); https://doi.org/10.1186/2193-8865-3-67
11. E. Kowsalya, *Food Packag. Shelf Life*, **21**, 100379 (2019); https://doi.org/10.1016/j.fpsl.2019.100379
12. E. Kowsalya, *J. Food Process Eng.*, **44**, e13641 (2021); https://doi.org/10.1111/jfpe.13641
13. S. Vigneswari, T.S.M. Amelia, M.H. Hazwan, G.K. Mouriya, K. Bhubalan, A.A. Amirul and S. Ramakrishna, *Antibiotics*, **10**, 229 (2021); https://doi.org/10.3390/antibiotics10030229
14. V.S. Parkhe, T.P. Patil and A.P. Tiwari, *Nanotechnol. Environ. Eng.*, **8**, 1067 (2023); https://doi.org/10.1007/s41204-023-00342-9
15. D. Bharathi, J. Lee, P. Karthiga, R. Mythili, S. Devanesan and M.S. AlSalhi, *Waste Biomass Valoriz.*, **15**, 1859 (2024); https://doi.org/10.1007/s12649-023-02328-9
16. C.G. Yuan, C. Huo, B. Gui and W.P. Cao, *IET Nanobiotechnol.*, **11**, 523 (2017); https://doi.org/10.1049/iet-nbt.2016.0183
17. S.K. Madhumithra, P. Balashanmugam, K. Mosachristas, A. Tamil Selvi and R. Subashini, *Int. J. Appl. Pharm.*, **10**, 162 (2018); https://doi.org/10.22159/ijap.2018v10i4.27154
18. K.X. Lee, K. Shameli, M. Miyake, N. Kuwano, N.B.B.A. Khairudin, S.E.B. Mohamad and Y.P. Yew, *J. Nanomaterials*, **2016**, 8489094 (2016); https://doi.org/10.1155/2016/8489094
19. E. Alzahrani and A.T. Alkhudidy, *Int. J. Anal. Chem.*, **719**, 2868 (2021); https://doi.org/10.1155/2021/7192868
20. E. Kowsalya, K. Mosa-Christas, C.R.I. Jaquline, P. Balashanmugam, and T. Devasena, *Appl. Organomet. Chem.*, **35**, e6071 (2020); https://doi.org/10.1002/aoc.6071
21. E. Iqbal, K.A. Salim and L.B.L. Lim, *J. King Saud Univ. Sci.*, **27**, 224 (2015); https://doi.org/10.1016/j.jksus.2015.02.003
22. T. Mosmann, *J. Immunol. Methods*, **65**, 55 (1983); https://doi.org/10.1016/0022-1759(83)90303-4
23. M. Uzma, N. Sunayana, V.B. Raghavendra, R. Shanmuganathan, C.S. Madhu, and K. Brindhadevi, *Process Biochem.*, **92**, 269 (2020); https://doi.org/10.1016/j.procbio.2020.01.019
24. V. Ramalingam, S. Revathidevi, T.S. Shanmuganayagam, R. Rajaram and L. Muthulakshmi, *Gold Bull.*, **50**, 177 (2017); https://doi.org/10.1007/s13404-017-0208-x
25. L. Wang, J. Xu, Y. Yan, H. Liu and F. Li, *Artif. Cells Nanomed. Biotechnol.*, **47**, 1216 (2019); https://doi.org/10.1080/21691401.2019.1593852
26. L. Jiang, H. Yu, C. Wang, F. He, Z. Shi, H. Tu, N. Ning, S. Duan and Y. Zhao, *Pharmaceuticals*, **15**, 1271 (2022); https://doi.org/10.3390/ph15101271
27. P. Balashanmugam, P. Durai, M.D. Balakumaran and P.T. Kalaichelvan, *J. Photochem. Photobiol. B*, **165**, 163 (2016); https://doi.org/10.1016/j.jphotobiol.2016.10.013
28. Y. Wang, X. He, K. Wang, X. Zhang and W. Tan, *Colloid. Surf. B*, **73**, 75 (2009); https://doi.org/10.1016/j.colsurfb.2009.04.027
29. B.S. Srinath and R.V. Rai, *J. Cluster Sci.*, **26**, 1483 (2015); https://doi.org/10.1007/s10876-014-0835-9
30. A.K. Mittal, Y. Chisti and U.C. Banerjee, *Biotechnol. Adv.*, **31**, 346 (2013); https://doi.org/10.1016/j.biotechadv.2013.01.003
31. N. Jara, N.S. Milán, A. Rahman, L. Mouheb, D.C. Boffito, C. Jeffryes and S.A. Dahoumane, *Molecules*, **26**, 4585 (2021); https://doi.org/10.3390/molecules26154585.
32. A.K. Singh and O.N. Srivastava, *Nanoscale Res. Lett.*, **10**, 1055 (2015); https://doi.org/10.1186/s11671-015-1055-4
33. R.E. Darienzo, O. Chen, M. Sullivan, T. Mironava and R. Tannenbaum, *Mater. Chem. Phys.*, **240**, 122143 (2020); https://doi.org/10.1016/j.matchemphys.2019.122143
34. R. Mansoori, F. Hataminia, S.M. Sadraei, S. Kharrazi and H. Ghanbari, *Nanomed. Res J.*, **8**, 383 (2023); https://doi.org/10.22034/nmrj.2023.04.007
35. Y. Wang, X. He, K. Wang, X. Zhang and W. Tan, *Colloids Surf. B Biointerfaces*, 73, 75 (2009); https://doi.org/10.1016/j.colsurfb.2009.04.027
36. M. Akhbari, R. Hajiaghaee, R. Ghafarzadegan, S. Hamedi and M. Yaghoobi, *IEE Nanobiotechnol.*, **17**, 100301 (2020); https://doi.org/10.1049/iet-nbt.2018.5040
37. R.T. Ariski, K.K. Lee, Y. Kimc and C.-S. Lee, *RSC Adv.*, **14**, 14582 (2024); https://doi.org/10.1039/D4RA00614C
38. X. Li, T. Ni and R. Xu, *J. Mol. Struct.*, **1294**, 136413 (2023); https://doi.org/10.1016/j.molstruc.2023.136413
39. P.B. Santhosh, J. Genova and H. Chamati, *Chemistry*, **4**, 345 (2022); https://doi.org/10.3390/chemistry4020026
40. A.A. Belew, S.H. Gebre, M.A. Assege, D.S. Meshesha and M.T. Ayana, *Results Chem.*, **18**, 102859 (2025); https://doi.org/10.1016/j.rechem.2025.102859
41. Y.S. Mostafa, S.A. Alamri, S.A. Alrumman, M. Hashem and Z.A. Baka. *Plants*, **10**, 2363 (2021); https://doi.org/10.3390/plants10112363
42. S. Jain, M. S. Mehata, *Sci. Rep.* **7**, 15867 (2017); https://doi.org/10.1038/s41598-017-15724-8
43. L. Rastogi, A.J. Kora and J. Arunachalam, *Mater. Sci. Eng. C*, **32**, 1571 (2012); https://doi.org/10.1016/j.msec.2012.04.044
44. A. Zuorro, A. Iannone, R. Lavecchia and S. Natali, *Chem. Eng. Trans.*, **81**, 1393 (2020); https://doi.org/10.3303/CET2081233
45. J. Anuradha, T. Abbasi and S.A. Abbasi, *J. Adv. Res.*, **6**, 711 (2015); https://doi.org/10.1016/j.jare.2014.03.006
46. P. AshaRani, M.P. Hande and S. Valiyaveettil, *BMC Cell Biol.*, **10**, 65 (2009); https://doi.org/10.1186/1471-2121-10-65
47. V.A. Patel, A. Longacre, K. Hsiao, H. Fan, F. Meng, J.E. Mitchell, J. Rauch, D.S. Ucker and J.S. Levine, *J. Biol. Chem.*, **281**, 4663 (2005); https://doi.org/10.1074/jbc.M508342200
48. C. Zhang and X. Shi, *Nanomedicine*, **15**, 1455 (2020); https://doi.org/10.2217/nnm-2020-0142
49. K. Rizwan, M. Zubair, N. Rasool, M. Riaz, M. Zia-Ul-Haq and V. De Feo, *Int. J. Mol. Sci.*, **13**, 6440 (2012); https://doi.org/10.3390/ijms13056440
50. K.W. Jung, Y.J. Won, C.M. Oh, H.J. Kong, D.H. Lee and K.H. Lee, *Cancer Res. Treat.*, **49**, 292 (2017); https://doi.org/10.4143/crt.2017.118
51. V. Kumar and S.K. Yadav, *J. Chem. Technol. Biotechnol.*, **84**, 151 (2009); https://doi.org/10.1002/jctb.2023
52. C.H. Lee, Y. Choi, H. Cho, I.H. Bang, L. Hao, S.O. Lee, R. Jeon, E.J. Bae and B.H. Park, *Biochem. Pharmacol.*, **183**, 114312 (2021); https://doi.org/10.1016/j.bcp.2020.114312
53. H. Chang, Q. Wang, X. Meng, X. Chen, Y. Deng, L. Li, Y. Yang, G. Song and H. Jia, *Chem. Res. Toxicol.*, **35**, 1435 (2022); https://doi.org/10.1021/acs.chemrestox.1c00402
54. M. Pradeep, D. Kruszka, P. Kachlicki, D. Mondal and G. Franklin, *ACS Sustainable Chem. Eng.*, **10**, 562 (2022); https://doi.org/10.1021/acssuschemeng.1c06960